Trypanosoma brucei metacaspase 4 is a pseudopeptidase and a virulence factor

William R Proto[1], Esther Castanys-Munoz[1], Alana Black[1], Laurence Tetley[1], Catherine X Moss[1], Luiz Juliano[2], Graham H Coombs[3], Jeremy C Mottram[1].

[1] Wellcome Trust Centre for Molecular Parasitology, Institute of Infection, Immunity and Inflammation, College of Medical, Veterinary and Life Sciences, University of Glasgow, Glasgow, G12 8TA

[2] Department of Biophysics, Universidade Federal de Sao Paulo, Escola Paulista de Medicina, Rua Tres de Maio, 100; 04044-020 São Paulo, Brazil

[3] Strathclyde Institute of Pharmacy and Biomedical Sciences, University of Strathclyde, Glasgow G4 ORE

Running title: *Metacaspase 4 is a pseudopeptidase virulence factor*

Corresponding author: Professor Jeremy C Mottram. 120 University Place, Glasgow G12 8TA. E-mail: jeremy.mottram@glasgow.ac.uk; Tel: +44 141 330 3745; Fax: +44 141 330 8269

Background: Metacaspases are multi-functional cysteine peptidases.

Results: *Trypanosoma brucei* metacaspase 4 is a catalytically inactive metacaspase homologue required for parasite virulence, which interacts with an active parasite metacaspase during release from the cell.

Conclusion: Metacaspase 4 is a pseudopeptidase virulence factor.

Significance: Extracellular release and proteolytic processing provide novel insights into metacaspase function.

SUMMARY
Metacaspases are caspase family cysteine peptidases found in plants, fungi and protozoa, but not mammals. *Trypanosoma brucei* is unusual in having five metacaspases (MCA1-MCA5) of which MCA1 and MCA4 have active site substitutions, making them possible non-enzymatic homologues. Here we demonstrate that recombinant MCA4 lacks detectable peptidase activity, despite maintaining a functional peptidase structure. MCA4 is expressed primarily in the bloodstream form of the parasite and associates with the flagellar membrane via dual myristoylation/palmitoylation. Loss of function phenotyping revealed critical roles for MCA4; rapid depletion by RNAi caused lethal disruption to the parasite's cell cycle, yet the generation of MCA4 null mutant parasites (Δ*mca4*) was possible. Δ*mca4* had normal growth in axenic culture, but markedly reduced virulence in mice. Further analysis revealed that MCA4 is released from the parasite and is specifically processed by MCA3, the only metacaspase that is both palmitoylated and enzymatically active. Accordingly we have identified that the multiple metacaspases in *T. brucei* form a membrane-associated proteolytic cascade to generate a pseudopeptidase virulence factor.

Metacaspases (MCAs) are clan CD, family C14B, cysteine peptidases identified in plants, fungi and protozoa (1). They are predicted to be structurally similar to caspases with a caspase/haemoglobinase fold and a canonical histidine and cysteine dyad in the active site (1). MCAs differ from caspases in that they lack Asp specificity having a strict arginine or lysine substrate specificity, and many are activated by calcium (2-4). Many MCAs undergo autocatalytic processing of the zymogen to produce a mature enzyme, although this processing is not necessarily required for enzymatic activity (2,4,5). The natural targets of MCAs are uncertain, with the proteolytic cleavage of *Picea abies* Tudor

staphylococcal nuclease (TSN) by the MCA mcII-Pa during embryogenesis and induced programmed cell death being the only *in vivo* action reported to date (6).

A seminal study that identified the *Saccharomyces cerevisiae* MCA (Yca1) as a positive regulator of programme cell death (7) sparked great interest and paved the way for many subsequent descriptions of additional pro-death roles for MCAs (8). However, sustained research on MCAs of various organisms has revealed that they represent a functionally diverse family of peptidases. The single MCAs of *S. cerevisiae* and *Leishmania major* apparently harbour a capacity for multi-functionality. Yca1 is implicated in both cell cycle regulation (9) and the clearance of insoluble protein aggregates (10), while the MCA of *L. major* (LmjMCA) is required for cell cycle progression (11) in addition to having a role in PCD induced by oxidative stress (12). Furthermore, the antagonistic relationship of two *Arabidopsis thaliana* MCAs in the hypersensitive response cell death pathway (AtMC1 promotes cell death, while AtMC2 functions as a negative regulator) reveals the potential of MCAs for complex connections in key regulatory processes (13).

Trypanosoma brucei unusually has five *MCA* genes (*MCA1-MCA5*), only three of which (*MCA2*, *MCA3* and *MCA5*) encode proteins with the canonical histidine-cysteine catalytic dyad and are therefore predicted to be catalytically active (14,15). Investigation into these MCAs revealed collective essentiality for bloodstream form parasites; simultaneous RNAi depletion caused rapid cell death attributed to accumulation of abnormal cell types resulting from a pre-cytokinesis defect (16). Despite this severe phenotype resulting from RNAi, triple null mutant parasites (Δ*mca2/3*Δ*mca5*) were generated and had similar growth in axenic culture and mice, as in wild type parasites. While questions remain regarding the precise role of these MCAs it appears that they are not required for prostaglandin D2 induced programme cell death (16). However, the three MCAs were found to be associated with RAB11-positive endosomes, even though they are not necessary for the known recycling processes performed by these endosomes

(16). Deciphering the nature of this association could be pivotal to elucidating the main function(s) of these MCAs.

An intriguing aspect of the *T. brucei* MCA family is the presence of the two genes predicted to encode catalytically inactive proteins: MCA1 lacks both the histidine and cysteine of the expected active site dyad, whereas MCA4 has a serine in place of the usual catalytic cysteine (14,15). Substitutions within the catalytic centre of enzyme homologues is widespread across protozoan and metazoan proteomes, and some non-enzymatic homologues have been shown to play key regulatory roles (17). Indeed, regulation of some peptidases is known to occur through related inactive homologues. For example, the activity of caspase-8 in the mammalian extrinsic apoptotic pathway is regulated by direct interaction with cFLIP$_L$, an inactive caspase-8 homologue (18). Also, growth factor signalling that is dependent on the intramembrane rhomboid peptidases is controlled by iRhoms (inactive rhomboid homologues) through substrate sequestration and subsequent removal via endoplasmic reticulum degradation (19). However, not all atypical active site configurations preclude peptidase activity, with mixed-catalytic type peptidases also capable of proteolysis. The poliovirus-type picornain C3 peptidases are instrumental in processing expressed viral proteins with proteolytic activity derived from a cysteine nucleophile operating within a classical serine peptidase fold (20). To date no proteins have been identified with proteolytic activity derived from a serine nucleophile in a caspase fold.

Thus several possible roles for MCA4 could be envisaged and we undertook a detailed characterisation of the enzyme with the aim of elucidating the part it plays as a member of the *T. brucei* MCA family. We found that despite the potentially catalytic serine residue in the MCA4 active site, the recombinant enzyme lacked peptidase activity towards a combinatorial peptide library and the specific activity towards Arg/Lys residues characteristic of metacaspases and thus is a pseudopeptidase. In addition, reverse genetics revealed MCA4 to have roles in both cell cycle progression and parasite virulence during mammalian infection. Moreover, we show that the

2

membrane-associated MCA4 is specifically processed during its release by the palmitoylated and so membrane-bound MCA3 and thus that they appear to comprise a MCA proteolytic cascade.

EXPERIMENTAL PROCEDURES

Plasmids - Unless otherwise stated all PCR reactions used *T. brucei* (strain 427) genomic DNA as an amplification template and all oligonucleotide sequences are listed in Supplementary Information Table S1. For MCA4 protein expression the coding sequence was amplified using OL2329 and OL2330 and cloned into the pET-28a(+) (Novagen) using *Nde*I and *Xho*I restriction sites, creating pGL1697. MCA4[S219C] protein expression plasmid was produced by site directed mutagenesis of MCA4 in pGL1697 using OL2605 and OL2606. For the MCA4 RNAi plasmid a unique 469 bp fragment was identified by TrypanoFAN:RNAit (http://trypanofan.path.cam.ac.uk/software/RNAit) amplified using OL2312 and OL2313, and cloned into *Hin*dIII and *Bam*HI sites in p2T7[ti] (21), creating pGL1695. For transfection into *T. brucei* pGL1695 was digested with *Not*I. For deletion of the MCA4 locus the 5' and 3' flanks of the MCA4 ORF were amplified by PCR using the primer pairs OL3245 (*Not*I) OL3246 (*Xba*I) and OL3247 (*Apa*I) OL3248 (*Apa*I and *Xho*I), respectively. Using *Not*I/*Xba*I and *Apa*I/*Xho*I the 5' and 3' flanks were sequentially ligated into pGL1689, creating the NEO MCA4 knockout construct named pGL1986. Exchange of resistance genes was achieved by excising a HYG gene from pGL1688 using *Bmg*BI and *Bgl*II and cloning into pGL1986 pre-digested with *Bmg*BI and *Bgl*II, generating pGL1985 the HYG MCA4 knockout construct. For transfection into *T. brucei* pGL1986 and pGL1985 were digested with *Not*I and *Xho*I. The ectopic re-expression of MCA4 was achieved by modification of p2628 (22). Firstly the following primer pairs were used for site directed mutagenesis to introduced *Nde*I (OL3047, OL3048) and *Bcl*I (OL3046, OL3055) restriction sites flanking the HYG gene, thereby allowing replacement with a BSD gene, cloned from pGL1466 using OL3049 and OL3050. The resulting construct was digested with *Xho*I and *Bam*HI (removing the YFP coding

sequence) and the MCA4 gene amplified using OL3403 and OL3404 was cloned in producing pGL2067. For the ectopic expression of MCA4-YFP the same BSD re-expression construct was digested with *Hind*III and *Bam*HI allowing insertion of MCA4 cloned without the stop codon using OL3397 and OL3398 to create, pGL2132. For re-expression of mutant forms of MCA4, pGL2067 was subject to site directed mutagenesis. To investigate MCA4 membrane association, a cytosolic MCA4 mutant was generated by removing the predicted N-myristoylation site, using OL3768 and OL3769, creating MCA4[G2A]. The active site mutant MCA4[S219C] was produced using OL2605 and OL2606. All site directed mutagenesis alterations were made using the Quick Change Mutagenesis Kit (Stratagene) according to manufacturer's instructions and confirmed by DNA sequencing.

Parasites - *T. brucei* Lister 427 were grown in culture as bloodstream form to a maximum cell density of 1×10^6 ml^{-1} at 37°C in 5 % carbon dioxide in HMI-9 media supplemented with 10 % heat-inactivated foetal calf serum, 10 % serum plus and 0.5 µg ml^{-1} penicillin-streptomycin solution (Sigma). Procyclic form were grown to a maximum cell density of 1×10^7 ml^{-1} at 27°C in 5 % carbon dioxide in SDM-79 medium supplemented with 10 % FCS and 0.5 µg ml^{-1} penicillin-streptomycin solution (Sigma). The genetic knockout of MCA4 was performed in bloodstream form *T. brucei* 427. The triple MCA null mutant cell line (Δ*mca2/3*Δ*mca5*) was generated and characterised previously (16). For animal infection assays, 1×10^5 cultured parasites were inoculated into ICR mice by intra peritoneal injection and the parasitemia monitored daily by haemocytometer cell count of mouse blood taken from a tail vein diluted in 0.83 % ammonium chloride. For infection experiments, groups of four mice were infected with trypanosomes taken directly from the same donor mouse.

T. brucei transfection - 1×10^7 mid-log cells were harvested by centrifugation at 1500 g for 10 minutes at 37°C. The cell pellet was resuspended in 100 µl Human T Cell Nucleofector Solution (Lonza), transferred to an electroporation cuvette and mixed with 10 µg of linearised DNA and

3

pulsed once on programme X-001 using the Human T Cell Nucleofector machine (Amaxa). After overnight recovery, selection of clones was achieved by limiting dilution with appropriate antibiotics 5 μg ml^{-1} hygromycin B (Calbiochem), 2.5 μg ml^{-1} G418 (Calbiochem), 2.5 μg ml^{-1} phleomycin (InvivoGen) and 10 μg ml^{-1} blasticidin (Calbiochem). RNAi analysis and the tetracycline induced expression of tagged transgenes was performed in bloodstream form 427 13-90 and procyclic form 427 29-13 cell lines (23). To induce RNAi or transgene expression 1 μg ml^{-1} tetracycline was added to the culture medium, with cells re-seeded at 1 x 10^5 ml^{-1} every 24 hours.

Fluorescence activated cell sorting (FACS) - To analyse the DNA content of *T. brucei*, cells were fixed overnight in 70% methanol 30% PBS, washed in 10 ml PBS and resuspended in 1ml of PBS supplemented with 10 μg ml^{-1} propidium iodide (Sigma), 10 μg ml^{-1} RNAse A (Sigma) and incubated at 37°C for 45 minutes, in the dark. FACS analysis was performed on a Becton Dickinson FACSCalibur. For each sample, 10,000 events (cells) were analysed. Data interpretation was performed using the CellQuestPro software (BD Biosciences).

Recombinant protein: expression and purification - The MCA4 protein expression vector (pGL1697) was transformed into BL21 Rosetta *Escherichia coli* (Stratagene) and bacteria were grown in Overnight Express TB Medium (Novagen) for 16 hours and lysed in Bacterial Protein Extraction Reagent (Pierce) supplemented with 10 μg ml^{-1} DNAse 1 (Sigma). HIS-MCA4 was purified by immobilised metal ion affinity chromatography on a column packed with Metal Chelate-20 (Poros). MCA4 was eluted in 1 ml fractions using 50 mM NaH$_2$PO$_4$, 300 mM NaCl, 0.5 M Imidazole pH 8.0, then buffer exchanged into 50 mM Tris pH 8 using a PD10 column (GE Healthcare) and 150 mM NaCl subsequently added.

Antibody production - Purified recombinant MCA4 was used as an antigen to raise a polyclonal antibody. Two chickens were immunised with recombinant MCA4 (four 250 μl inoculations of 1 mg ml^{-1} protein over four months) at the Scottish National Blood Transfusion Service

(Penicuik, Midlothian). Total IgY was purified from egg yolks using the Eggcellent IgY Purification kit (Pierce), then affinity purified against recombinant MCA4 immobilised on AminoLink Coupling Gel (Pierce) according to manufacturer's instructions.

Immunoblotting - Whole cell extracts and purified proteins were mixed with LDS Sample Buffer (Invitrogen), denatured by heating at 100°C for 4 minutes, then electrophoresed on 12 % (w/v) SDS-PAGE. Gels were either stained with Coomassie Brilliant Blue R-250 (2.5 % (w/v)), 45 % (v/v) methanol, 10 % acetic acid) or transferred to nitrocellulose membrane (Hybond-C, Amersham Biosciences) for western blotting. Primary antibodies against MCA4, EF-1α (Millipore), Bip (gift from J.D.Bangs University of Wisconsin, Madison, WI, USA) were used at 1:800, 1:2000 and 1:15000 respectively. HRP-conjugated anti-chicken (Invitrogen) was used at 1:4000 and anti-mouse (Promega), anti-rabbit (Promega) and anti-sheep (Santa Cruz) were used at 1:5000. The cellular fractionation was verified using antibodies specific to the cytoskeletal protein β-tubulin (24) (KMX-1 monoclonal Millipore) diluted 1:10,000 and the cytoplasmic protein oligopeptidase B 1:1000 (25-27). Chemiluminescence detection was with the SuperSignal system or Novex ECL (Invitrogen).

Enzyme Assays - For autocatalytic processing 10 μg of purified recombinant MCA4 or MCA4^{S219C} was incubated in a reaction buffer (50mM Tris-HCl, pH 8, 150 mM NaCl, 5 mM DTT) with and without 10 mM CaCl$_2$ for 1 hour at 37°C. For MCA3 autocatalytic processing 5 μg of recombinant enzyme was incubated in described buffer supplemented with 1 mM CaCl$_2$. The extent of autocatalytic processing was monitored by SDS-PAGE. For MCA2 processing of MCA4 10 μg of purified MCA4 was incubated with increasing amounts of purified recombinant MCA2 (0, 1, 10 and 100 ng) in reaction buffer (50mM Tris-HCl, pH 8, 150 mM NaCl, 5 mM DTT, 10 mM CaCl$_2$) for 1 hour at 37°C. The extent of processing was monitored by SDS-PAGE.

Fluorogenic enzyme assays - Proteolytic activity of purified recombinant protein was assessed by measuring the

4

hydrolysis of synthetic fluorogenic substrates. All assays were run in clear bottom 96 well plates and typically contained the following components: 2 µg purified enzyme, reaction buffer (50mM Tris-HCl, pH 8, 150 mM NaCl, 5 mM DTT and 10 mM CaCl$_2$), 10 µM substrate (e.g. Z-RR-AMC) and distilled water to 200 µl. All assays were run in triplicate and included 'no-enzyme' controls. Fluorescence was read in an EnVision Multilabel Reader (Perkin Elmer, Beaconfield, UK) at excitation wavelength (λ_{Ex}) of 355 nm and emission wavelength (λ_{Em}) of 460 nm using the general mirror. Specific activities were calculated using a 7-amino-4-methylcoumarin standard (AMC). A positional-scanning combinatorial library was used to confirm the lack of MCA4 activity; Abz-GXXZXXQ-EDDnp, where Abz is *ortho*-aminobenzoic acid, Q-EDDnp is glutamine (ethylene diamine [2,4-dinitrophenyl]), the Z position was filled with 1 of 19 amino acids (cysteine was omitted), and X represents randomly incorporated amino acids.

Acyl-biotin exchange - To detect MCA4 palmitoylation an acyl biotin exchange assay was used as previously described by Emmer and co-workers (28).

N-terminal Edman degradation - To sequence the N-terminus of processing products reactions were set up as described above, electrophoresed on NuPAGE Novex 10 % Bis-Tris gels (Invitrogen) and transferred to a PVDF membrane (Hybond-P, Amersham Biosciences). Edman sequencing was performed by the University of Dundee, MRC Protein Phosphorylation Unit.

Microscopy - Images were obtained using an Applied Precision DeltaVision Deconvolution microscope system fitted with a CoolSnap HQ camera. Image capture and microscope operation was performed using the software package SoftWoRx. Fluorescence was viewed using the FITC filter (λ_{Ex} 490 nm / λ_{Em} 528 nm), RD-TR-PE filter (λ_{Ex} 555 nm / λ_{Em} 617 nm), DAPI filter (λ_{Ex} 360 nm / λ_{Em} 457 nm) and reference images were obtained using the differential interference contrast (DIC) filter. Exposure time was set to 1 second with the transmission level of the neutral filter optimised for each sample and 60x or 100x

oil immersion objectives were used. Typically 15 Z-stacks were obtained and individually deconvolved using the automatic conservative ratio setting before projection into one representative image. To merge images containing multiple fluorescent signals Adobe photoshop was used. For direct cell fluorescence, approximately 1 x 10^5 *T. brucei* were washed twice in trypanosome dilution buffer (TDB) (20 mM Na$_2$HPO$_4$, 2 mM NaH$_2$PO$_4$, 80 mM NaCl, 5 mM KCl, 1 mM MgSO$_4$, 20 mM glucose, pH 7.4) before fixation in 1 % (w/v) paraformaldehyde (Sigma) with concurrent incubation on ice for 15 minutes. After two further washes in TDB the cell pellet was resuspended in 20 µl TDB and evenly spread onto twin frosted end 76 x 26 mm microscope slide coated in 0.1 % poly-l-lysine (Sigma) and the cells allowed to sediment. Excess liquid was removed and the cells on each slide were stained with 10 µl of 1 µg ml^{-1} 4,6-Diamindino-2-phenylindole (DAPI) in mounting solution (PBS, 50 % (v/v) glycerol, 2.5 % (w/v) DABCO). All slides were fitted with a coverslip sealed with nail varnish.

Immunofluorescence analysis - The protocol used for immunofluorescence analysis was adapted from the method published by Field and co-workers (29). Briefly, mid-log bloodstream form parasites were washed in vPBS (137 mM NaCl, 3 mM KCl, 16 mM Na$_2$HPO$_4$, 3 mM KH$_2$PO$_4$, 46 mM sucrose, 10 mM glucose, pH 7.6) before fixation on ice in 3 % paraformaldehyde for 10 minutes. The fix solution was diluted out with excess vPBS and two further cell washes were performed. Fixed cells were applied to a 2 cm^2 area outlined in nail varnish, on 0.1 % poly-l-lysine treated microscope slides and allowed to sediment. When required the cells were permeabilised by applying 0.1 % (v/v) Triton X-100 in PBS for 10 minutes before washing with PBS and blocking for 1 hour using 20 % (v/v) foetal calf serum (Sigma) in PBS. Anti-MCA4 (1:400) diluted in blocking solution was applied and incubated for 2 hours at room temperature. Slides were washed three times with PBS before one incubation with Alexa Fluor 488 (green)-conjugated anti-chicken (Molecular Probes) diluted 1:7500 in blocking solution. Slides were washed three times with PBS, stained with 1 µg ml^{-1}

DAPI in mounting solution and sealed with a coverslip and nail varnish.

Immunoelectron microscopy - A bloodstream form *T. brucei* cell pellet was chemically fixed in suspension and maintained in 0.2 % (v/v) gluteraldehyde, 2 % (w/v) paraformaldehyde in PBS (pH 7.2) on ice for 1 hour. After fixation the cells were rinsed in PBS and embedded in Lowicryl resin using the progressive lowering of the temperature method. Cells were cut into blocks and mounted on metal pins and frozen in liquid nitrogen before sectioning with a Leica Ultracut UCT/FCS. The cryosections were blocked with 0.1 M glycine followed by 5 % (w/v) BSA and then labelled with affinity purified anti-MCA4 (1:10) and 1.4 nm gold (rabbit) anti-chicken (1:20) (Aurion). Cells were contrast stained and the immuno-labelling was enhanced by 15 minutes treatment with R-gent (Aurion). Sections were viewed with a LEO 912 transmission electron microscope.

Cell fractionation - The cellular fractionation method was adapted from (30). For detergent lysis 2×10^7 mid-log cells were washed in vPBS and lysed in 500 μl 1% (v/v) Triton X-100, 25mM HEPES, 1mM EDTA pH7.4 for 30 mins on ice before centrifugation at 14,000 g for 5 min. For hypotonic lysis 2×10^7 mid-log BSF cells were washed in vPBS and lysed in 500 μl 10mM Tris-HCl pH7.4 with 4×15 second blasts in an ice cold sonicating water bath (Fisher Scientific FB15047), before centrifugation at 14,000 g for 5 minutes. For both lysis methods, insoluble material in the pellet was solubilised by boiling with 625 μl 1 x SDS-PAGE sample buffer for 5 min. The supernatant was prepared for electrophoresis by adding 125 μl 4 x SDS-PAGE sample buffer and boiling for 5 min. 1×10^6 cell equivalents were loaded per lane.

Motility analysis - *T. brucei* resistance to sedimentation was investigated as a function of cell motility (31). Wild type BSF *T. brucei* and Δ*mca4* cells were cultured to the same mid-log densities. 2 ml of culture was divided equally into 2 cuvettes and the OD_{600} was recorded at 0, 3 and 6 hour time points. One cuvette remained undisturbed and the other mixed and re-suspended before each optical density reading. Three replicate experiments were performed and sedimentation rates determined by subtracting the OD_{600} of the undisturbed control from the OD_{600} of the resuspended culture.

MCA4 Release - To detect release of MCA4 1×10^8 mid-log *T. brucei* cells were washed in TDB and incubated at 37°C in 15 ml 50% serum free HMI9 50% TDB. Cell viability was monitored every hour by haemocytometer count and after 3.5 hours cells were removed by centrifugation at 1500 x g for 15 minutes. Trypanosome free medium was carefully aspirated and Complete Protease Inhibitor Cocktail (Roche) added to final concentration of 1.5 x, before slow passage through 0.2 μm syringe filter and 75-fold concentration using a VivaSpin 20 10,000 MWCO filter unit. The concentrated supernatant was prepared for SDS-PAGE and 35 μl loaded alongside whole cell lysate from 1×10^5 cells and electrophoresed on a 12% SDS-PAGE, then transferred to nitrocellulose for western blotting.

Statistical analysis of data - Where indicated data were expressed as means ± standard deviation from the mean. P-values were calculated using an unpaired, two-tailed Student's T-test on Microsoft Excel. Differences were considered significant at a p-value of <0.001.

RESULTS

MCA4 is a pseudopeptidase - The predicted active site of MCA4 maintains the canonical histidine residue but has serine instead of the usual cysteine nucleophile (14,15). Given the highly specific nature of enzyme active sites, it seemed likely that this substitution would make the peptidase inactive. However, other possibilities existed. Firstly, it is possible MCA4 functions as a mixed-type peptidase utilising the reactive hydroxyl group of the serine as a nucleophile. Secondly, two cysteine residues widely conserved amongst MCAs but located outside of the predicted active site may serve as alternative catalytic residues; MCA4 Cys98 is found in all MCAs and MCA4 Cys218 is present in all kinetoplast MCAs (14,32). Thus, we first sought to establish whether or not MCA4 is an active peptidase through analysis of the recombinant protein.

6

Previous work demonstrated that TbMCA2 undergoes rapid calcium-dependent autocatalytic processing but that this is not required for activity (2). MCA4 remained unprocessed in the presence of calcium (Fig. 1A) and a range of peptide substrates cleaved by MCA2, including Z-GGR-AMC, Z-GRR-AMC, Z-RR-AMC and a peptide library containing all amino acids in the P1 position, also failed to detect MCA4 activity. An MCA4^{S219C} mutant, in which the active site serine was replaced with cysteine, was, however, capable of autoprocessing when incubated with calcium (Fig. 1B). N-terminal Edman sequencing of the major proteolytic processing product identified autocatalytic cleavage at Lys64 (KESK^{64}GFQPWK). Consistent with metacaspase-specificity towards basic residues in the P1 position we found that MCA4^{S219C} could also cleave the peptide substrate Z-GGR-AMC, although at a rate greatly reduced in comparison to MCA2 (MCA2 11 ± 3.0; MCA4^{S219C} 0.031 ± 0.0043 mU/mg protein). MCA4^{S219C} activity was similar to that of MCA2 in being dependent on calcium and strongly inhibited by leupeptin and antipain but only mildly inhibited by E64 (Fig. 1C). These data collectively demonstrate that creation of the canonical metacaspase-dyad in MCA4 produces a calcium-dependent proteolytically active enzyme, confirming that MCA4 has retained the structure of active MCAs; the lack of peptidase activity, however, means that it is a pseudopeptidase.

RNAi depletion of MCA4 severely restricts parasite proliferation - Western blot analysis revealed that MCA4 expression has a distinct stage-specificity, with the protein being present in the bloodstream form but not detectable in the procyclic form of the parasite (Fig. 2A). The antibody specificity was confirmed by analysis of an *MCA2*, *MCA3*, *MCA5* triple null mutant (16), in which the immunopositive band was similar in intensity to that in wild type parasites (Fig. 2A). The size of the MCA4 protein in the parasite extracts was very close to the predicted 40 kDa molecular mass of the full length protein, showing that under standard *in vitro* growth conditions MCA4 in the parasite was not subject to detectable proteolytic processing events.

This defined pattern of expression suggested an important role specific to bloodstream forms, so in order to investigate this we characterized the effects of targeted RNAi downregulation of MCA4 in this life cycle stage. Following RNAi induction, a rapid growth arrest occurred at around 8 hours with only low numbers of motile cells persisting over the remainder of the RNAi time course (Fig. 2B). Western blot analysis was used to verify the successful depletion of MCA4 (Fig. 2C). To analyse the progression of RNAi-induced parasites through the cell cycle, the configuration of nuclei (N) and kinetoplasts (K) was determined by fluorescent microscopy of DAPI-stained cells (Fig. 2D). The reduction of cells with one nucleus and one kinetoplast (1N1K cells) with increased 2N2K and abnormal cells (classified as 'others' including those containing increased DNA content and zoids) showed that induced cells were able to replicate their DNA but failed to correctly execute cytokinesis. The flow cytometry profiles of the induced cells confirmed the DAPI analysis (Fig. *S1*). These RNAi data suggest that MCA4 is essential for the normal proliferation of bloodstream form *T. brucei*. This finding corroborates and expands upon a similar observation following a genome-wide RNAi silencing screen which identified MCA4 as having a loss of fitness phenotype (33).

An important role for MCA4 in virulence - Previous work demonstrated that simultaneous RNAi silencing of MCA2, MCA3 and MCA5 was lethal to bloodstream form *T. brucei*, yet the generation of triple null mutant cell lines was still possible (16). We found this was also the case with MCA4, as *MCA4* null mutants (Δ*mca4*) were readily generated. MCA4 and a number of mutant MCA4 re-expression lines were created through introduction of specific amino acid changes within MCA4 (designated Δ*mca4:MCA4*, Δ*mca4:MCA4*^{G2A} and Δ*mca4:MCA4*^{S219C}). The validity of the genetic manipulation was confirmed by Southern blotting (Fig. *S2*) and western blotting was used to verify the absence of MCA4 in Δ*mca4* cells and to demonstrate re-expression occurred at an equivalent level to the wild type cells (Fig. 3A).

The initial growth rate of Δ*mca4* parasites in culture was greatly reduced in

comparison with the parental wild type strain (Fig. *S3*). However, following several weeks of continuous growth and sub-culturing, the growth rate of Δ*mca4* recovered and DAPI analysis revealed that, unlike the RNAi-induced cells, no major defects were detected in cell cycle progression or motility (Fig. S3).

A potential role of MCA4 in the mammalian infection process was investigated by comparing the infection profiles of wild type and mutant parasites in mice. The wild type parasites were highly virulent in mice and by day 4 established parasitemia above 10^8 cells ml^{-1}, which was when the mice were culled (Figs. 3B and 3C). Δ*mca4* parasites, however, showed a drastically different infection profile, with mouse survival prolonged to around 15 days (Fig. 3B). The reduced *in vivo* growth rate of MCA4-deficient parasites could be partially restored by the re-expression of MCA4, with 75 % of mice succumbing to Δ*mca4:MCA4* infection by day 7. Axenic culture of parasites isolated from mice at the first peak of parasitemia revealed normal growth for all strains (Fig. S3) indicating the variation observed *in vivo* was due to interaction with the host.

Detailed analysis of the parasitemia patterns of the infected mice revealed several interesting trends. The wild type parasites were extremely virulent and the parasitemia increased very rapidly (Fig. 3C). In contrast, mice infected with Δ*mca4* had a peak of parasitemia separated by a trough period where parasitemia was below the detection threshold. In the re-expression cell lines, the parasitemia profile was more similar to that of the wild type cells, typified by consistent growth with only one mouse per group being able to very briefly clear infection to below the detection threshold (Fig. 3C).

MCA4 associates with the flagellar membrane - The cellular localisation of MCA4 was revealed by immunofluorescence microscopy using affinity-purified, anti-MCA4 antibody (Fig. 4A). MCA4 was found to localise predominantly to the flagellum, appearing as a combination of punctate structures and larger confluent foci distributed along the entire length of the flagellum. This was confirmed by re-expression of MCA4 with a C-terminal yellow fluorescent protein (YFP) fusion in Δ*mca4* parasites, which also revealed a distinct flagellum localisation when viewed by direct fluorescent microscopy. Immunogold transmission electron microscopy studies provided further detailed evidence supporting the punctate nature of MCA4 along the flagellum, with the enhanced immunogold particles appearing in clusters at unmarked but distinct foci along the internal surface of the flagellum (Fig. 4B).

The *T. brucei* flagellum is a complex organelle composed of multiple distinct structures. To gain potential insights into MCA4 function, the precise location within the flagellum was assessed using a subcellular fractionation procedure capable of distinguishing between soluble, cytoskeletal and membrane-associated proteins. Western blot analysis of *T. brucei* subcellular fractions demonstrated that MCA4 was a membrane-associated protein, being found in the pellet of the hypotonic and sonicated cell lysate and the soluble fraction of the detergent treated cell lysate (Fig. 5A). To verify the quality of the fractionation procedure, the different fractions were probed with antibodies specific to the cytoskeletal protein β-tubulin and the cytoplasmic protein oligopeptidase B. To determine whether MCA4 was located on the internal or external surface of the flagellar membrane, immunofluorescence microscopy was performed in the presence and absence of Triton X-100 (Fig. 4A). The stronger staining of the flagellum was detected in those cells treated with detergent, suggesting that the MCA4 epitopes were mainly internally located and required permeabilisation for exposure.

No single flagellar-targeting sequence has been identified for *T. brucei*, however dual acylation has been shown to influence the flagellar membrane association of several proteins (28,34,35). Previous comprehensive bioinformatic screens identified MCA4 Gly-2 as a target for N-myristoylation (36), a modification often associated with palmitoylation. Accordingly we attempted to provide experimental evidence of *in vivo* MCA4 palmitoylation using an acyl-biotin exchange reaction (28). Western blotting of material from the experimental and control reactions revealed

8

that MCA4 was purified in a hydroxylamine-dependent manner from *T. brucei* cell lysate, confirming the protein was palmitoylated *in vivo* (Fig. 5B). This experimental finding combined with the bioinformatic predictions suggests that MCA4 is dually acylated.

The influence of acylation on MCA4 localisation was investigated by creation of a MCA4[G2A] mutation that was predicted to prevent N-myristoylation and consequently palmitoylation. MCA4[G2A] was re-expressed in Δ*mca4* parasites and fractionation of the Δ*mca4:MCA4*[G2A] parasites revealed that MCA4[G2A] appeared in the soluble material following hypotonic lysis (Fig. 5A). Immunofluorescent analysis of the Δ*mca4:MCA4*[G2A] mutants showed that MCA4[G2A] was dispersed throughout the cytoplasm and absent from the flagellum (Fig. 4A). Infection of mice with Δ*mca4:MCA4*[G2A] parasites demonstrated complementation of the Δ*mca4* phenotype, indicating that under the condition tested flagellar membrane localisation of MCA4 is not essential for an effect on the parasite's virulence (Figs 3B, 3C).

Processing of MCA4 and release - Previous work identified MCA4 as part of the secretome of two independent *T. brucei gambiense* strains (37). We therefore tried to provide independent verification of a similar occurrence in *T. brucei*. Cultured mid-log phase bloodstream form parasites were incubated in serum-free medium for 3.5 hours before removal by centrifugation. The resulting parasite-free medium was concentrated and analysed alongside whole cell lysate by western blot. MCA4 was clearly evident in the released material, appearing as different sized proteins; a higher molecular mass species (identical in size to the protein detected in cell lysate) and two smaller less abundant processed forms (Fig. 6A). Non-specific protein accumulation in the medium was analysed by probing the blot with anti-Bip which is largely retained intracellularly (38). In comparison to the parasite lysate, only small amounts of Bip were detected in the released material (Fig. 6A). MCA4 release was detected in both Δ*mca4:MCA4* and Δ*mca4:MCA4*[G2A] cell lines, revealing MCA4 release occurred independent of flagellar membrane localisation (Fig. 6A). One key finding, however, was the absence of any processed MCA4 protein in the material released from Δ*mca4:MCA4*[G2A] cells. This excluded the possibility of random degradation of MCA4 occurring in the medium and suggested a specific proteolytic event dependent upon association of MCA4 with the flagellar membrane.

To test if one of the other TbMCAs might be responsible for MCA4 processing, we analysed material released from Δ*mca2/3* Δ*mca5* parasites (16) and found that only full length MCA4 could be detected. We analysed individual re-expressor cell lines and identified MCA3 as the major peptidase responsible for MCA4 processing (Fig. 6A). MCA2 and MCA3 proteins share 89% sequence identity with near identical catalytic domains and divergence only found at the N-terminus (15,16), a difference that does not appear to alter the enzyme's substrate specificity (Fig. S4). Thus it was intriguing that *in vivo* processing of MCA4 was mediated only by MCA3. To rule out the possibility that MCA4 is resistant to MCA2 proteolytic activity we incubated recombinant MCA4 with MCA2 (2:1 molar ratio) and, having confirmed that it had no significant impact on MCA2 activity, showed that recombinant MCA2 processed MCA4 with a similar pattern of cleavage as the autocatalytic processing by MCA4[S219C] (compare Figs 6B and 1B). N-terminal Edman degradation revealed that processing occurred at Lys64, the same residue cleaved during autocatalytic processing of recombinant MCA4[S219C] (Figs 1B and 6B). These data suggest that the selective *in vivo* proteolytic cleavage of MCA4 by MCA3 must be due to reasons other than specificity per se and provide direct evidence that there is co-localisation of and interaction between these *T. brucei* MCAs in a proteolytic cascade resulting in release of the pseudopeptidase.

DISCUSSION

The active site residues of metacaspases have been identified through sequence alignment and homology with caspases, followed in some cases by experimental verification (2,4). The predicted active site of MCA4 is of particular interest due to the presence of a potential serine nucleophile within a

cysteine peptidase. Here we demonstrate, however, that MCA4 does not have autocatalytic activity, or activity towards a range of peptide substrates, ruling out the possibilities that it functions as a mixed type peptidase or that catalytic activity can be derived from other conserved cysteine residues. Nevertheless, by using mutagenesis to reinstate a canonical-metacaspase active site we have shown that MCA4^{S219C} has calcium-dependent MCA-like activity and consequently the native protein has retained a functional peptidase tertiary structure. In light of these findings, we speculate that the active site cysteine was mutated in an ancestral MCA, generating the pseudopeptidase MCA4, which now fulfils an important role for the parasite.

Targeted RNAi down-regulation indicated that MCA4 is essential for bloodstream form cell proliferation. At 24 hours post-induction, abnormal cell types accumulated which is indicative of a post-mitotic block and links MCA4 to a role in cytokinesis. However, the MCA4 RNAi mutants broadly conform to a common phenotype associated with the RNAi down-regulation of key bloodstream form flagellar proteins (39). Therefore, given the flagellar membrane association that we have demonstrated for MCA4, we predict that MCA4 is more likely to exert its effect on cytokinesis indirectly.

The implied essentiality of MCA4 following RNAi down-regulation strongly suggested that the gene would be refractory to genetic deletion. However, *MCA4* was successfully deleted from bloodstream form cells creating viable null mutant parasites (Δ*mca4*). We attribute this apparent discrepancy to the differing dynamics of MCA4 depletion associated with each technique. RNAi of MCA4 leads to rapid removal of the protein preventing parasite adaptation, whereas the sequential replacement of each allele during creation of the null mutants provides sufficient time for parasite adjustment to diminishing MCA4 levels. This adaptation in null mutants has also been described for Δ*mca2/3*Δ*mca5* parasites (16). In that instance, it was suggested that MCA4 may be an alternative compensatory biochemical pathway following the deletion of MCA2, MCA3 and MCA5. However, given the absence of

MCA4 activity and the markedly different localisation this now appears unlikely.

The ancestral MCA homologue in *T. brucei* is likely to be MCA5, given its synteny with the single *L. major* MCA. This raises the question of whether MCA function differs between organisms with a single metacaspase (such as budding yeast and *L. major*) and organisms with multiple MCAs (*T. brucei* and *A. thaliana*). MCA2, MCA3 and MCA4 are all expressed at a higher level in the bloodstream form of the parasite than in the procyclic form, whereas MCA5 is expressed equally in both life cycle stages ((16) and this study). Accordingly, we speculated that MCA4 could be involved in trypanosome-specific functions associated with mammalian infectivity. Indeed, infection of mice with wild type *T. brucei* and Δ*mca4* cell lines revealed strikingly different patterns of infection; with Δ*mca4* cells showing periods below the detection threshold and consecutive days of reduced parasite burdens more similar to pleomorphic bloodstream form strains than to the parental highly virulent monomorphic 427 strain. This resulted in a markedly extended survival time for the host mice and revealed a role for MCA4 in parasite virulence within the mammalian host.

Our data, together with a recent characterisation of the flagellum proteome (40) has identified a flagellum localisation for MCA4. Several other flagellar proteins have also been shown to influence *T. brucei* virulence in mice. The deletion of the GPI-phospholipase C created a prolonged infection in mice that was accompanied by multiple peaks and troughs of parasitemia (41). In addition, *in vivo* RNAi silencing of the calflagins (Tb17, Tb24 and Tb44) prolonged mouse survival by attenuating parasite growth, creating an infection with waves of parasitemia associated with the expression of alternative variant surface glycoproteins (42). Although not confirmed experimentally, it seems likely that the reduced virulence of Δ*mca4* allowed the host's immune system sufficient time to clear the original infection before the re-emergence of cells expressing a different VSG type.

Regulated proteolytic activity is an important mechanism of signal transduction used by peptidases to modify properties of

10

substrate proteins. The strict specificity displayed by many Clan CD peptidases is dictated by a highly selective S1 pocket, which ensures they are well adapted to carry out specific processing events and less suited to perform random proteolytic degradation. This is well demonstrated by the many complex and intricate signalling pathways involving caspases during their participation in apoptosis and inflammation (43). Indeed, related processes have recently been reported for a MCA from *Picea abies* (mcII-Pa) that was shown to inactivate a tudor staphylococcal nuclease (TSN) protein through cleavage at four defined sites during programmed cell death events associated with embryogenesis and oxidative stress (6). However, whether this represents a highly specific form of signal transduction, as witnessed for capsases, is open to some debate (8). Our observation that MCA3 processes MCA4 provides the first identification of an *in vivo T. brucei* MCA substrate, which is only the second MCA substrate to be identified, after TSN (6). While the biological significance of MCA4 processing is unknown, this cleavage event establishes an important link between two MCAs that may be a component of a broader MCA cascade. Moreover, the proteolytic inactivity of MCA4 suggests it lies at the end of any such proteolytic cascade. This arrangement, whereby MCA4 is placed under the control of MCA3, may optimise release and action of MCA4 in a highly regulated manner.

The major form of MCA4 detected after release from the parasite was similar in size to the full length protein, but less abundant lower molecular mass forms were also detected. As re-expression of MCA4^{G2A} in Δ*mca4* resulted in the release of only the full length protein, processing of MCA4 is clearly dependent upon correct membrane localisation and was not the product of random degradation or autocatalytic activity. Our finding that MCA3 processes MCA4 is particularly relevant as MCA3 has been reported to be present in RAB11 positive endosomes/exosomes (16) and the flagellum proteome (40) and is the only other *T. brucei* MCA that is palmitoylated (35). These data suggest that there must be some cross-over between the exosome membranes and the flagellum, at which point MCA4 is processed and released. We have also shown that lipidation is crucial in allowing direct interaction between MCA3 and MCA4 on the membrane. However, this interaction at the membrane is not essential for the release of MCA4, as the non-lipidated mutant is also released, possibly via an alternative route.

The way in which MCA4 exerts its influence upon infection in a mammalian host remains to be established, but the recent proposal that exosome release, by both intracellular and extracellular pathogens, can allow effector molecule delivery to host cell cytosol (44), provides a possible mechanism for delivery of trypanosome virulence factors (45). Our finding that MCA4 is released by bloodstream form *T. brucei* and does not appear to influence the processing or activity of other MCAs, opens up the possibility that it could target and regulate host molecules. Future investigation of *T. brucei* strains that establish natural chronic infections could help identify potential MCA4 interactions and allow further clarification of its role in parasite virulence.

11

REFERENCES

1. Uren, A. G., O'Rourke, K., Aravind, L., Pisabarro, M. T., Seshagiri, S., Koonin, E. V., and Dixit, V. M. (2000) *Mol Cell* **6,** 961-967
2. Moss, C. X., Westrop, G. D., Juliano, L., Coombs, G. H., and Mottram, J. C. (2007) *FEBS Letts* **581,** 5635-5639
3. Watanabe, N. and Lam, E. (2005) *J Biol Chem* **280,** 14691-14699
4. Vercammen, D., van de Cotte, B., De Jaeger, G., Eeckhout, D., Casteels, P., Vandepoele, K., Vandenberghe, I., Van Beeumen, J., Inzé, D., and Van Breusegem, F. (2004) *J Biol Chem* **279,** 45329-45336
5. Bozhkov, P. V., Suarez, M. F., Filonova, L. H., Daniel, G., Zamyatnin, A. A., Rodriguez-Nieto, S., Zhivotovsky, B., and Smertenko, A. (2005) *Proc Natl Acad Sci USA* **102,** 14463-14468
6. Sundstrom, J. F., Vaculova, A., Smertenko, A. P., Savenkov, E. I., Golovko, A., Minina, E., Tiwari, B. S., Rodriguez-Nieto, S., Zamyatnin, A. A., Valineva, T., Saarikettu, J., Frilander, M. J., Suarez, M. F., Zavialov, A., Stahl, U., Hussey, P. J., Silvennoinen, O., Sundberg, E., Zhivotovsky, B., and Bozhkov, P. V. (2009) *Nat Cell Biol* **11,** 1347-1354
7. Madeo, F., Herker, E., Maldener, C., Wissing, S., Lächelt, S., Herlan, M., Fehr, M., Lauber, K., Sigrist, S. J., Wesselborg, S., and Fröhlich, K. U. (2002) *Mol Cell* **9,** 911-917
8. Tsiatsiani, L., Van Breusegem, F., Gallois, P., Zavialov, A., Lam, E., and Bozhkov, P. V. (2011) *Cell Death Differ* **18,** 1279-1288
9. Lee, R. E. C., Puente, L. G., Kaern, M., and Megeney, L. A. (2008) *Plos One* **3,** e2956
10. Lee, R. E. C., Brunette, S., Puente, L. G., and Megeney, L. A. (2010) *Proc Natl Acad Sci USA* **107,** 13348-13353
11. Ambit, A., Fasel, N., Coombs, G. H., and Mottram, J. C. (2007) *Cell Death Differ* **15,** 113-122
12. Zalila, H., Gonzalez, I. J., El Fadili, A. K., Delgado, M. B., Desponds, C., Schaff, C., and Fasel, N. (2011) *Mol Microbiol* **79,** 222-239
13. Coll, N. S., Vercammen, D., Smidler, A., Clover, C., Van Breusegem, F., Dangl, J. L., and Epple, P. (2010) *Science* **330,** 1393-1397
14. Szallies, A., Kubata, B. K., and Duszenko, M. (2002) *FEBS Letts* **517,** 144-150
15. Mottram, J. C., Helms, M. J., Coombs, G. H., and Sajid, M. (2003) *Trends Parasitol* **19,** 182-187
16. Helms, M. J., Ambit, A., Appleton, P., Tetley, L., Coombs, G. H., and Mottram, J. C. (2006) *J Cell Sci* **119,** 1105-1117
17. Pils, B. and Schultz, J. (2004) *J Mol Biol* **340,** 399-404
18. Yu, J. W., Jeffrey, P. D., and Shi, Y. (2009) *Proc Natl Acad Sci USA* **106,** 8169-8174
19. Zettl, M., Adrain, C., Strisovsky, K., Lastun, V., and Freeman, M. (2011) *Cell* **145,** 79-91
20. Sarkany, Z. and Polgar, L. (2003) *Biochemistry* **42,** 516-522
21. LaCount, D. J., Bruse, S., Hill, K. L., and Donelson, J. E. (2000) *Mol Biochem Parasitol* **111,** 67-76
22. Kelly, S., Reed, J., Kramer, S., Ellis, L., Webb, H., Sunter, J., Salje, J., Marinsek, N., Gull, K., Wickstead, B., and Carrington, M. (2007) *Mol Biochem Parasitol* **154,** 103-109
23. Wirtz, E., Leal, S., Ochatt, C., and Cross, G.A. (1999) *Mol Biochem Parasitol* **99,** 89-101
24. Birkett, C. R., Foster, K. E., Johnson, L., and Gull, K. (1985) *FEBS Letts* **187,** 211-218
25. Burleigh, B. A., Caler, E. V., Webster, P., and Andrews, N. W. (1997) *J Cell Biol* **136,** 609-620
26. Morty, R. E., Lonsdale-Eccles, J. D., Mentele, R., Auerswald, E. A., and Coetzer, T. H. T. (2001) *Infect Immun* **69,** 2757-2761
27. Munday, J. C., McLuskey, K., Brown, E., Coombs, G. H., and Mottram, J. C. (2011) *Mol Biochem Parasitol* **175,** 49-57
28. Emmer, B. T., Souther, C., Toriello, K. M., Olson, C. L., Epting, C. L., and Engman, D. M. (2009) *J Cell Sci* **122,** 867-874
29. Field, M. C., Allen, C. L., Dhir, V., Goulding, D., Hall, B. S., Morgan, G. W., Veazey, P., and Engstler, M. (2004) *Microsc Microanal* **10,** 621-636

30. Liu, W., Apagyi, K., McLeavy, L., and Ersfeld, K. (2010) *Mol Biochem Parasitol* **169,** 20-26

31. Bastin, P., Pullen, T. J., Sherwin, T., and Gull, K. (1999) *J Cell Sci* **112,** 3769-3777

32. Belenghi, B., Romero-Puertas, M. C., Vercammen, D., Brackenier, A., Inzé, D., Delledonne, M., and Van Breusegem, F. (2007) *J Biol Chem* **282,** 1352-1358

33. Alsford, S., Turner, D. J., Obado, S. O., Sanchez-Flores, A., Glover, L., Berriman, M., Hertz-Fowler, C., and Horn, D. (2011) *Genome Res* **21,** 915-924

34. Absalon, S., Blisnick, T., Kohl, L., Toutirais, G., Dore, G., Julkowska, D., Tavenet, A., and Bastin, P. (2008) *Mol Biol Cell* **19,** 929-944

35. Emmer, B. T., Nakayasu, E. S., Souther, C., Choi, H., Sobreira, T. J. P., Epting, C. L., Nesvizhskii, A. I., Almeida, I. C., and Engman, D. M. (2011) *Eukaryot Cell* **10,** 455-463

36. Mills, E., Price, H. P., Johner, A., Emerson, J. E., and Smith, D. F. (2007) *Mol Biochem Parasitol* **152,** 22-34

37. Geiger, A., Hirtz, C., Becue, T., Bellard, E., Centeno, D., Gargani, D., Rossignol, M., Cuny, G., and Peltier, J. B. (2010) *BMC Microbiol* **10,** 20

38. Bangs, J. D., Brouch, E. M., Ransom, D. M., and Roggy, J. L. (1996) *J Biol Chem* **271,** 18387-18393

39. Broadhead, R., Dawe, H. R., Farr, H., Griffiths, S., Hart, S. R., Portman, N., Shaw, M. K., Ginger, M. L., Gaskell, S. J., Mckean, P. G., and Gull, K. (2006) *Nature* **440,** 224-227

40. Oberholzer, M., Langousis, G., Nguyen, H. T., Saada, E. A., Shimogawa, M. M., Jonsson, Z. O., Nguyen, S. M., Wohlschlegel, J. A., and Hill, K. L. (2011) *Mol Cell Proteomics* In press,

41. Webb, H., Carnall, N., Vanhamme, L., Rolin, S., Abbeele, J. V. D., Welburn, S., Pays, E., and Carrington, M. (1997) *J Cell Biol* **139,** 103-114

42. Emmer, B. T., Daniels, M. D., Taylor, J. M., Epting, C. L., and Engman, D. M. (2010) *Eukaryot Cell* **9,** 934-942

43. Pop, C. and Salvesen, G. S. (2009) *J Biol Chem* **284,** 21777-21781

44. Silverman, J. M. and Reiner, N. E. (2011) *Cell Microbiol* **13,** 1-9

45. Grébaut, P., Chuchana, P., Brizard, J. P., Demettre, E., Seveno, M., Bossard, G., Jouin, P., Vincendeau, P., Bengaly, Z., Boulangé A., Cuny, G., and Holzmuller, P. (2009) *Int J Parasitol* **39,** 1137-1150

FOOTNOTES

Abbreviations: MCA, metacaspase; TSN, tudor staphylococcal nuclease; mcII-Pa, *Picea abies* metacaspase; Yca1, *S. cerevisiae* metacaspase; cFLIP$_L$, cellular FLICE-like inhibitory protein long form; Bip, endoplasmic reticulum hsp70 protein, binding protein.

FIGURE LEGENDS

FIGURE 1. MCA4 and MCA4^{S219C} peptidase activity. (*A*) Lack of calcium dependent MCA4 autoprocessing (10 μg) was analysed by SDS-PAGE. (*B*) Calcium dependent MCA4^{S219C} (10μg) autoprocessing was analysed by SDS-PAGE. The N-terminus of the major processed product was sequenced and the processing site marked with an asterisk. (*C*) Cleavage of Z-GGR-AMC by 5 μg MCA4^{S219C} was measured in conditions indicated, expressed as relative value and given as mean ± standard deviation.

FIGURE 2. MCA4 expression and analysis by RNAi. (*A*) Total cell lysates were prepared from *T. brucei* bloodstream form (lane 1) and procyclic form (lane 2) and bloodstream form Δ*mca2/3*Δ*mca5* (lane 3) and separated by SDS-PAGE before western blotting with anti-MCA4. An antibody specific to EF-1α demonstrates equal loading. (*B*) MCA4 RNAi in bloodstream form was induced by 1 μg ml^{-1} tetracycline (Tet+) and parasite growth rate compared to non-induced control (Tet-). (*C*) Western blot analysis of MCA4 protein level during RNAi time course. (*D*) The effect of MCA4 RNAi on cell cycle progression was determined by assessing DNA configuration using DAPI staining and fluorescence microscopy. >200 cells were counted per time point. Cells at the start of the cycle with a single nucleus (N) and kinetoplast (K) are 1N1K. Kinetoplast division occurs ahead of nuclear division, leading to 1N2K cells before post mitotic 2N2K cells. Those cells with abnormal DNA content classified as 'other'.

FIGURE 3. Analysis of bloodstream form MCA4 null mutants. (*A*) Western blot of Δ*mca4* and re-expression cell lines. Lane 1, *T. brucei* 427; Lane 2, Δ*mca4*; Lane 3, Δ*mca4:MCA4*; Lane 4, Δ*mca4:MCA4*^{G2A}; Lane 5 Δ*mca4:MCA4*^{S219C}. (*B*) Groups of 4 mice were infected with 3 x 10^5 parasites (2 mice for wild type parasites) and mouse survival was monitored daily and is shown by a Kaplan-Meier survival curve. (*C*) Mice were infected with 3 x10^5 parasites and parasitemia was monitored by tail prick and haemocytometer cell count. Mice were culled when parasitemia reached >1 x 10^8 cells ml^{-1} or upon presentation of severe symptoms.

FIGURE 4. Localisation of MCA4 in bloodstream form trypanosomes. (*A*) Immunofluorescence. Cells were permeabilized with Triton X-100 or left intact, before incubation with anti-MCA4 antibody and anti-chicken Alexa Fluor 488 conjugate, visualised using FITC filter set (green). DNA stained with DAPI (blue) and reference images taken with differential interference contrast (DIC) filter settings. Scale bars 5 μm. (*B*) MCA4 immunogold transmission electron microscopy. Fixed cells were cryosectioned and labelled with anti-MCA4 and 1.4 nm gold conjugated rabbit anti-chicken. Black arrowheads show enhanced immunogold particles. Lower left image represent digitally magnified section of the corresponding image above, arrow head labelled a and b are labelled a' and b' on magnified section.

FIGURE 5. Subcellular fractionation and modification of MCA4 in bloodstream form trypanosomes. (*A*) Cell fractionation. Total cell lysate (T), detergent soluble (DS), detergent pellet (DP), hypotonic soluble (HS) and hypotonic pellet (HP) fractions were analysed by western blot using anti-MCA4 antibody. Quality of fractionation was validated with antibodies specific to β-tubulin and OPB. (*B*) Acyl-biotin exchange reaction. Palmitoylated proteins were specifically labelled by cleaving palmitate-thioester bonds with hydroxylamine and subsequently reacted with biotin-HPDP allowing purification with streptavidin agarose. Original cell lysate (I), the wash fraction (W) and eluted material (E) from hydroxylamine treated and Tris control samples were immunoblotted with anti-MCA4 antibody.

FIGURE 6. MCA4 release and proteolytic processing by MCA3 (*A*) Detection of MCA4 in released material. Cells were incubated in serum free medium then removed by centrifugation before concentration of cell free fraction and analysis by western blot. Total cell lysate (T) and released material (R) was probed with anti-MCA4. The blot was stripped and reprobed with anti-Bip. (*B*) MCA4 processing by MCA2 was analysed by SDS-PAGE. The N-terminus of the major processed product was sequenced and six amino acids were identified (underlined) and the cleavage site marked with an asterisk. RB; reaction buffer.

14

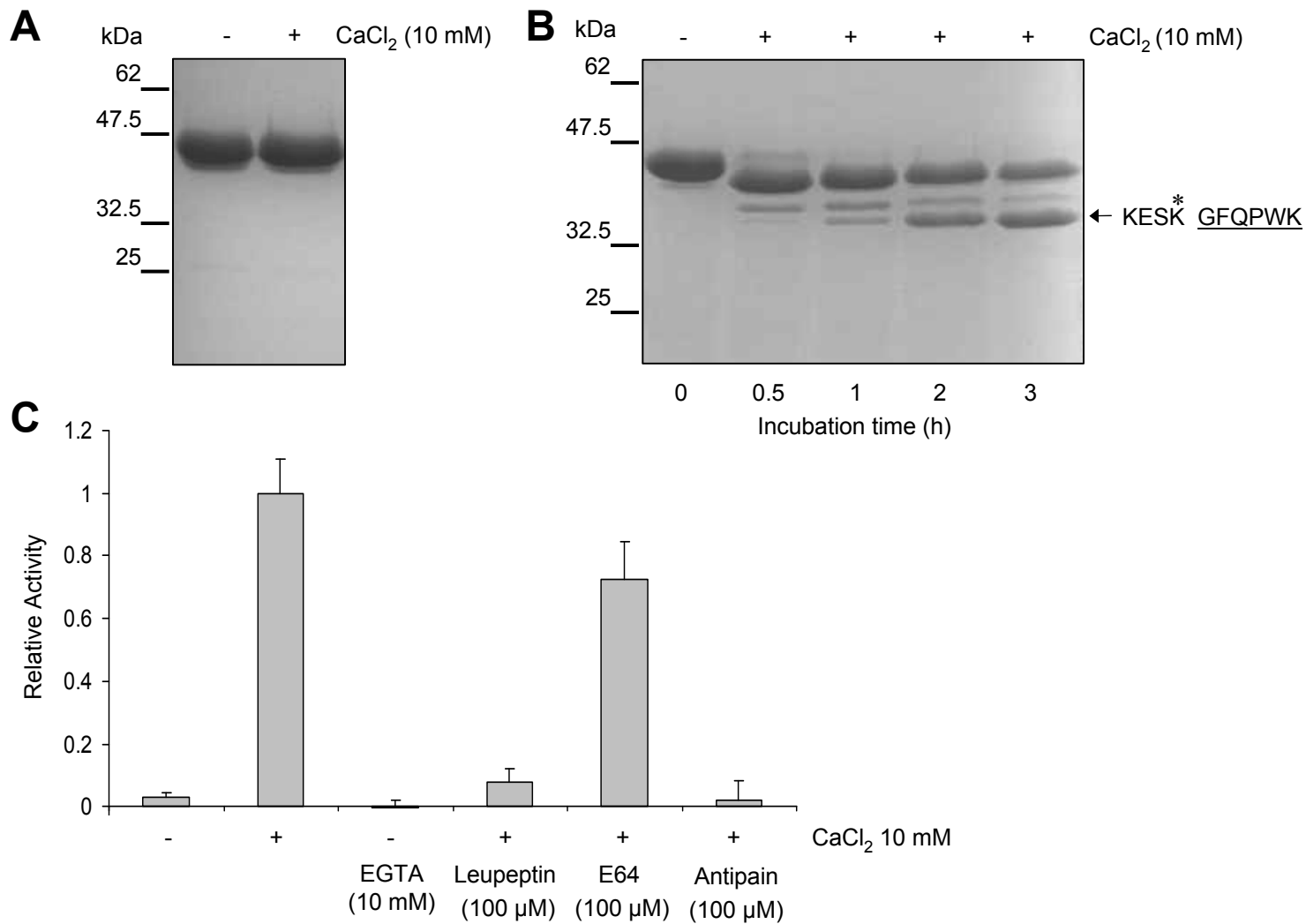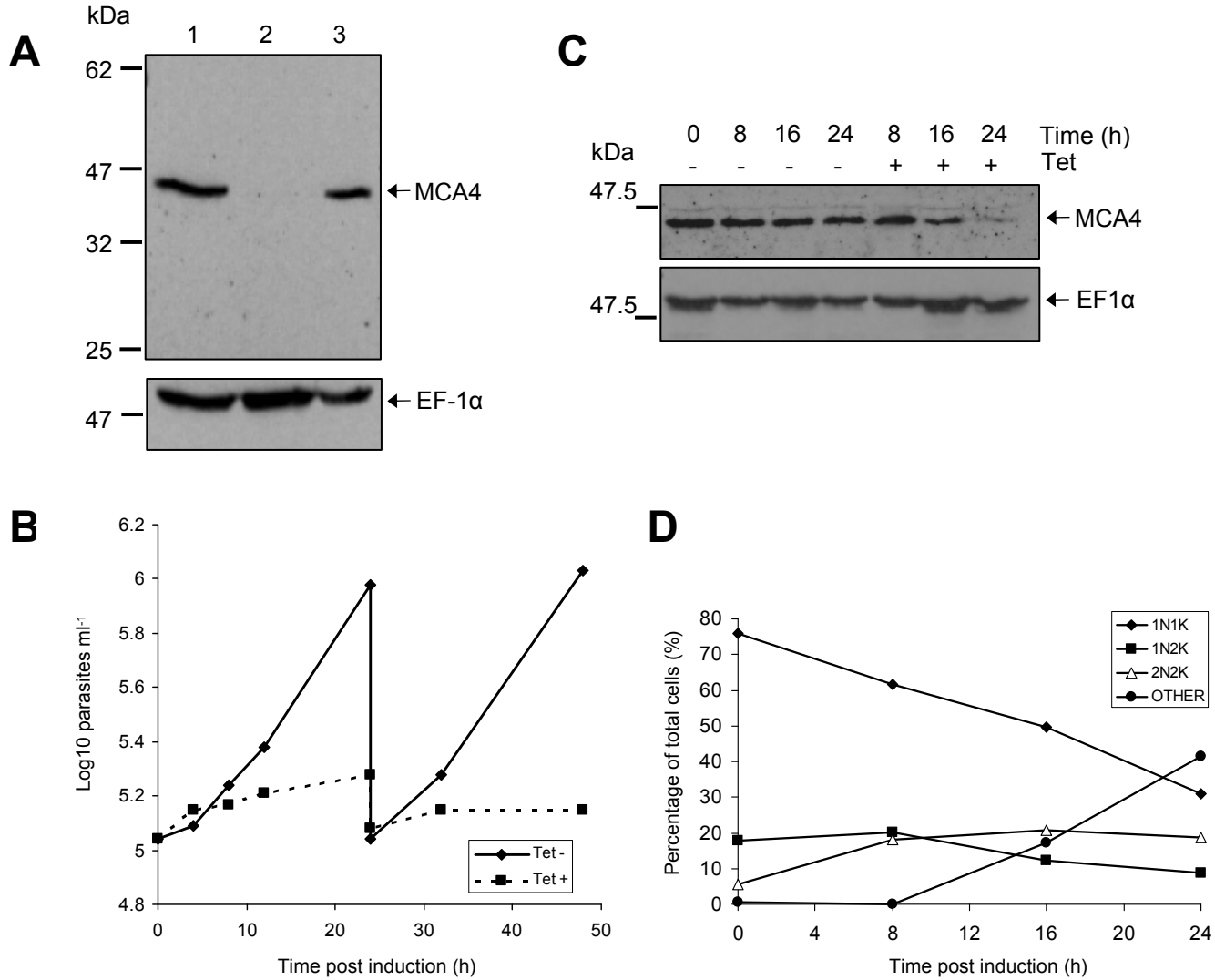**Figure 1**

A

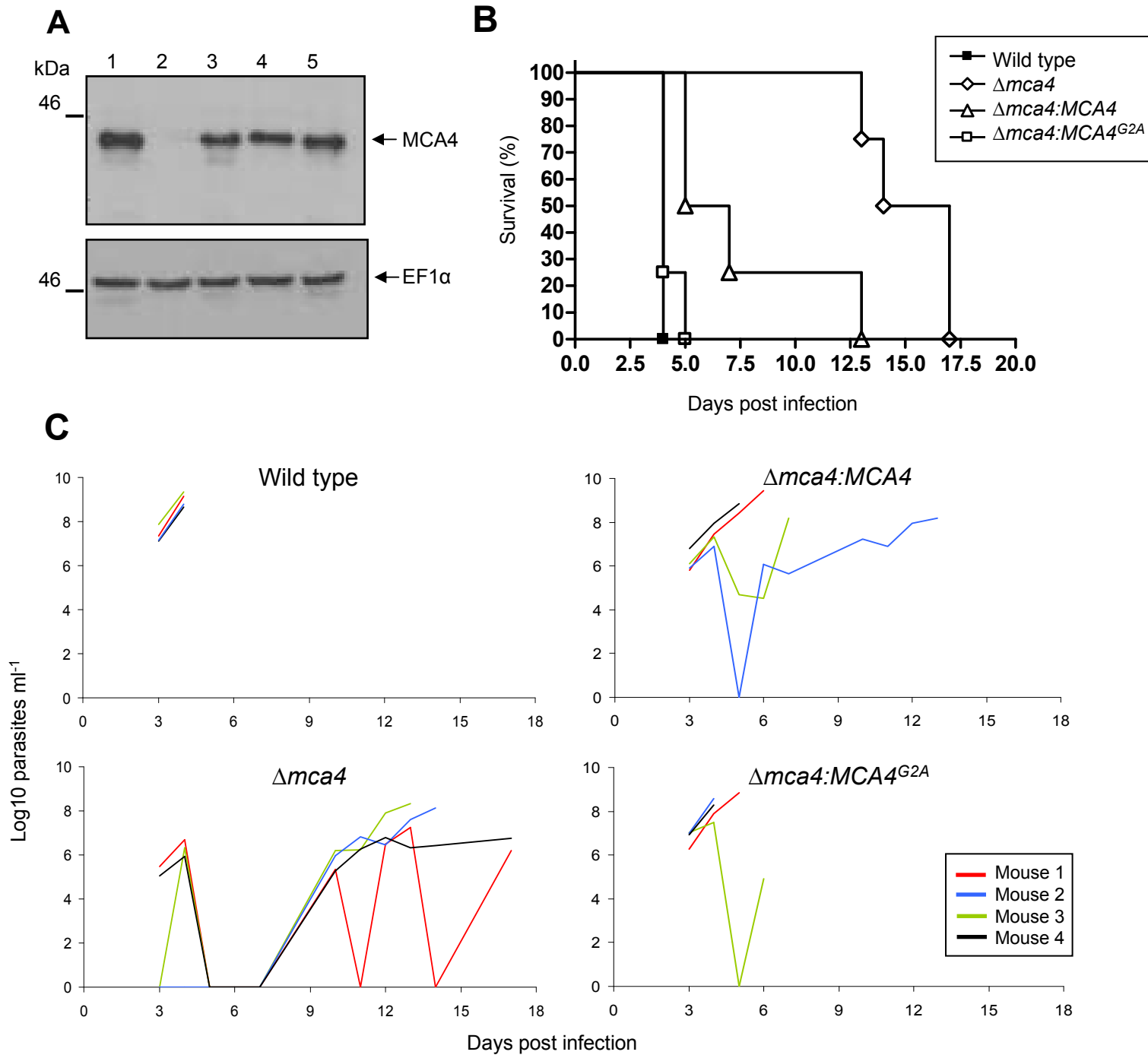kDa   -   +   CaCl$_2$ (10 mM)

62
47.5
32.5
25

B

kDa   -   +   +   +   +   CaCl$_2$ (10 mM)

62
47.5
32.5
25

← KESK* GFQPWK

0   0.5   1   2   3

Incubation time (h)

C

Relative Activity

1.2
1
0.8
0.6
0.4
0.2
0

-    +   -   +   +   +   CaCl$_2$ 10 mM

EGTA   Leupeptin   E64   Antipain
(10 mM)   (100 μM)   (100 μM)   (100 μM)

Figure 2

Figure 3

Figure 4

A

| Wild type | Wild type | Δ*mca4* | Δ*mca4*:MCA4 | Δ*mca4*:MCA4^{G2A} | Δ*mca4*:YFP-MCA4 |

- Triton X-100 |———————————————— + Triton X-100 ————————————————|

B

A

	T	DS	DP	HS	HP		T	DS	DP	HS	HP	

kDa

46 ___

← MCA4

58 ___

← β-tubulin

80 ___

← OPB

Wild type   Δ*mca4:MCA4^{G2A}*

B

kDa   I   W   E

47.5 ___

← MCA4

Hydroxylamine

I   W   E

47.5 ___

← MCA4

Tris control

Figure 5

Figure 6

A

B